In situ observation of atmospheric oxygen and carbon dioxide in the North Pacific using a cargo ship

Yu Hoshina[1], Yasunori Tohjima[1], Keiichi Katsumata[1], Toshinobu Machida[1], and Shin-ichiro Nakaoka[1]

[1]National Institute for Environmental Studies, Tsukuba, 305-8506, Japan

Correspondence to: Yu Hoshina (hoshina.yu@nies.go.jp)

Abstract. Atmospheric oxygen (O_2) and carbon dioxide (CO_2) variations in the North Pacific were measured aboard a cargo ship, the *New Century 2* (NC2), while it cruised between Japan and the United States between December 2015 and November 2016. A fuel cell analyzer and a non-dispersive infrared analyzer were used for measurement of O_2 and CO_2, respectively. To achieve parts-per-million precision for the O_2 measurements, we precisely controlled the flow rates of the sample and reference air introduced into the analyzers and the outlet pressure. A relatively low airflow rate (10 cm^3 min^{-1}) was adopted to reduce the consumption rate of the reference gases. In the laboratory, the system achieved measurement precisions of 3.8 per meg for the $\delta(O_2/N_2)$, which is commonly used to express atmospheric O_2 variation, and 0.1 ppm for the CO_2 mole fraction. After the *in situ* observation started aboard NC2, we found that the ship's motion caused false wavy variations of the O_2 signal with an amplitude of more than several tens of ppm and a period of about 20 s. Although we have not resolved the problem at this stage, hourly averaging considerably suppressed the variation associated with ship motion. Comparison between the *in situ* observation and flask sampling of air samples aboard NC2 showed that the averaged differences (*in situ* – flask) and the standard deviations (±1σ) are −2.8±9.4 per meg for the $\delta(O_2/N_2)$ and −0.02±0.33 ppm for the CO_2 mole fraction. We compared one year of *in situ* data for atmospheric potential oxygen (APO) (= O_2 + 1.1 × CO_2) obtained from the broad middle-latitudes region (140°E–130°W, 29°N–45°N) with previous flask sampling data from the North Pacific. This comparison showed that longitudinal differences in the seasonal amplitude of APO, ranging from 51 to 73 per meg, were smaller than the latitudinal differences.

1 Introduction

The balance of CO_2 emissions from fossil fuel combustion, land biotic CO_2 uptake, and ocean CO_2 uptake determines long-term change in the atmospheric CO_2 burden. At the same time, fossil fuel combustion consumes atmospheric O_2 while the land biotic CO_2 uptake is accompanied by emission of O_2 into the atmosphere. Additionally, today's ocean is considered to be a weak source of O_2 because of recent ocean warming (Bopp et al.,

2002; Keeling and Garcia, 2002; Plattner et al., 2002). The CO_2 and O_2 exchanges for biotic processes and fossil fuel combustion are stoichiometrically related, and the fossil fuel consumption rate can be reliably estimated from energy statistics. Therefore, coupled measurements of the atmospheric CO_2 and O_2 have been used to constrain the global CO_2 budgets by simultaneously solving the equations for the atmospheric CO_2 and O_2 budgets (Keeling and Shertz, 1992; Battle et al., 2000, 2006; Manning and Keeling, 2006; Tohjima et al., 2008; Ishidoya et al., 2012).

Atmospheric O_2 measurements are also useful for understanding air-sea gas exchange. This is based on the fact that the air-sea exchange of O_2 is more than one order of magnitude faster than that of CO_2; chemical equilibrium of the dissolved inorganic carbon (dissolved CO_2, bicarbonate and carbonate ions) in seawater suppresses the air-sea exchange of CO_2 (e.g., Keeling et al., 1993). For example, seasonality in the ocean biotic activity and the sea surface temperature is poorly reflected in air-sea CO_2 exchange, while oceanic O_2 fluxes show clear seasonal variations. The role of atmospheric O_2 as a tracer of air-sea gas exchange is emphasized by the introduction of the tracer atmospheric potential oxygen (APO), which is defined as $APO = O_2 + 1.1 \times CO_2$ (Stephens et al., 1998), where 1.1 represents the $-O_2/CO_2$ exchange ratio associated with land biotic activity (Severinghaus, 1995). Since APO is invariant with respect to the land biotic O_2 and CO_2 exchange and predominantly reflects the air-sea gas exchange, spatiotemporal variations in APO have been used to study gas fluxes associated with ocean ventilation (Lueker et al., 2003) and ocean spring bloom (Yamagishi et al., 2008) to estimate net ocean production (Keeling and Shertz, 1992; Balkanski et al., 1999; Nevison et al., 2012) and to validate ocean biogeochemical models (Stephens et al., 1998; Naegler et al., 2007; Nevison et al., 2008, 2015, 2016).

The precision required to detect atmospheric O_2 variation is at the μmol/mol (ppm) level, which is considerably smaller than the atmospheric O_2 mole fraction of about 21%. Keeling (1988) was the first to develop an atmospheric O_2 measurement technique with this precision, using an interferometer and showing the usefulness of O_2 measurements to study the global carbon cycle. Since then, several O_2 measurement techniques based on a mass spectrometer (Bender et al., 1994), a paramagnetic analyzer (Manning et al., 1999), a fuel cell analyzer (Stephens et al., 2007), and a vacuum ultraviolet absorption photometer (Stephens et al., 2003) have been developed and applied to atmospheric observations (cf. Keeling and Manning, 2014). When the change in atmospheric O_2 concentration is compared with that of CO_2, it is expressed as a deviation of the O_2/N_2 ratio from an arbitrary reference according to

$$\delta(O_2/N_2) = \frac{(O_2/N_2)_{sam}}{(O_2/N_2)_{ref}} - 1 \quad (1)$$

where subscripts *sam* and *ref* represent sample and reference gases, respectively, and the $\delta(O_2/N_2)$ value is usually converted to a "per meg" value, which approximates parts per million, by multiplying it by 10^6 (Keeling and Shertz, 1992). The mole fraction is not used as a measure of O_2 abundance because the changes in the mole fraction of major atmospheric constituents like O_2 are sometimes very confusing. For example, adding 1 μmol of O_2 to an air parcel containing 1 mol of dry air results in a 0.79-ppm increase in the O_2 mole fraction and adding 1 μmol of CO_2 results in not only a 1-ppm increase in the CO_2 mole fraction but also a 0.21-ppm decrease in the O_2 mole fraction. These confusing results are attributed to influences of the changes in the total number of moles in the air parcel on the mole fractions or dilution effect (e.g., Keeling et al., 1998; Tohjima 2000). However, adding 1 μmol of O_2 to 1 mol of dry air, which contains 0.2094 mol of O_2 (Tohjima et al., 2005), always results in a 4.77-per meg change in the $\delta(O_2/N_2)$ value.

The National Institute of Environmental Studies, Japan (NIES) also developed a technique to measure the atmospheric O_2 based on a gas chromatograph equipped with a thermal conductivity detector (GC/TCD) (Tohjima, 2000). NIES began measuring atmospheric O_2 and CO_2 by collecting air samples in glass flasks at two monitoring stations, Hateruma Island in July 1997 and Cape Ochi-ishi in December 1998 (Tohjima et al., 2003, 2008). Additionally, to extend the observation area, we started flask sampling aboard cargo ships sailing between Japan and Australia/New Zealand (Oceanian route) and between Japan and North America (North American route) in December 2011 (Tohjima et al., 2005, 2012). Moreover, *in situ* measurements of the atmospheric O_2 using the GC/TCD technique also started aboard a cargo ship between Japan and Australia/New Zealand in 2007 (Yamagishi et al., 2012).

These O_2 and CO_2 data from widespread Pacific regions were used to investigate the spatial distribution of the climatological seasonal cycle of APO and the annual mean values of APO (Tohjima et al., 2012). Latitudinal transects of the data in the western Pacific region revealed that variation in the magnitude of the bulge in annual mean APO was associated with the El Niño–Southern Oscillation cycle (Tohjima et al., 2015). This analysis was made possible by the relatively high spatiotemporal sampling density in the western Pacific. In contrast, the spatiotemporally sporadic APO data obtained from the North American route made it difficult to investigate interannual variations in the northern and eastern North Pacific. In 2015, Pickers et al. (2017) started *in situ* observations of atmospheric O_2 and CO_2 with a fuel cell analyzer and non-dispersive infrared analyzer aboard a commercial container ship regularly traveling in the Atlantic Ocean between Hamburg, Germany, and Buenos Aires, Argentina. They also showed the usefulness of continuous observation to reveal the spatiotemporal APO

distribution. Therefore, in December 2015, we initiated a program of *in situ* measurements aboard a cargo ship, the *New Century 2* (NC2) sailing between Japan (Tahara port) and North America.

Since June 2014, atmospheric greenhouse gas measurements, including flask sampling (7 flasks per round trip), have been conducted aboard NC2 along the North American route in the Pacific. We also had an opportunity to install an atmospheric O_2 measurement system aboard NC2. However, since the aboard space allotted to us was limited, we had to make the measurement system smaller by reducing the number of cylinders required for the system. In addition, since it is difficult to load and unload high-pressure gas cylinders on ocean-going ships, we needed to reduce the consumption rate of reference gases to reduce the cylinder exchange frequency. With these constraints, the GC/TCD technique, which requires at least 16 m^3 of He as a carrier gas for 1 yr of continuous O_2 observation, was unsuitable for use aboard NC2. Therefore, we developed a low-flow system to perform *in situ* atmospheric O_2 and CO_2 measurements aboard NC2. In this paper, we present details of the measurement system and report its fundamental performance in laboratory testing. We also discuss a problem that occurred when the measurement system was installed aboard NC2. Finally, we present 1 yr of atmospheric O_2, CO_2, and APO data and discuss the longitudinal distribution of the seasonal APO cycle in the North Pacific.

2 Methods

2.1 Analytical system

Figure 1 is a schematic diagram of the *in situ* observation system used aboard NC2. We used a fuel cell analyzer (Oxzilla-II, Sable System, USA) and a non-dispersive infrared analyzer (LI-840A, LI-COR, USA) for the aboard measurement of O_2 and CO_2, respectively. After passing a polypropylene cartridge filter with a mesh size of 7 μm (MCP-7-C10S, ADVANTEC, Japan), the sample air is drawn by a diaphragm pump (MOA-P108-HB, Gast Mfg. Corp., USA) at a flow rate of about 8×10^3 cm^3 min^{-1} and introduced into a spherical glass vessel with a volume of about 2×10^3 cm^3. The air is vented to the atmosphere through a back-pressure regulator (6800AL, KOFLOC, Japan), which keeps the pressure inside the spherical vessel at about 0.05 MPa above ambient pressure. Water that condenses within the spherical vessel is drained from the bottom by a peristaltic pump (7016-21, Masterflex, USA). The sample gas for the O_2 and CO_2 measurements is drawn from the center of the spherical vessel through 1/16-inch stainless steel (SUS) tubing. The technique of sampling from a spherical glass vessel was adopted to reduce fractionation of the O_2/N_2 ratio (Yamagishi et al., 2008).

The gas sampled from the spherical vessel is introduced into a two-stage cold trap (−80°C) to reduce the water vapor concentration to less than 1 ppm. Details of the cold trap are presented in Section 2.2. The dried sample gas and working reference gas, which is supplied from a high-pressure cylinder, are introduced into the two fuel cells of the O_2 analyzer via two mass flow controllers (SEC-E40MK3, HORIBA STEC, Japan) and a 4-way 2-position valve (AC4UWE, Valco Instruments Co. Inc., USA). The mass flow controllers regulate the flow rates of the two gas streams with a precision of 0.01 cm^3 min^{-1}. The dried sample air and working reference air alternately pass through each fuel cell at intervals of 2 min by switching the 4-way 2-position valve. The CO_2 analyzer is placed downstream of one of the fuel cells. The flow rates of the outflows from the CO_2 analyzer and the other fuel cell are monitored by mass flow meters (SEF-E40, HORIBA STEC, Japan) with a precision of 0.01 cm^3 min^{-1}. We adjusted the settings of the mass flow controllers until the readings of the mass flow meters for the two air streams matched. The outflows of the mass flow meters are combined and vented to the atmosphere via a piezo actuator valve (PV-1202MC, HORIBA STEC, Japan). The outlet pressures of the analyzers are kept at the same absolute value at all times by actively matching them to a reference pressure using the piezo actuator valve and a differential pressure sensor (Model 204, Setra Systems, USA).

Before the dried sample gas is introduced into the mass flow controller, it passes through a multi-position valve (EMTCSD6MWM, Valco Instruments Co. Inc., USA), to which three standard gases are connected. During the calibration procedures, the multi-position valve selects the standard gases instead of the sample air, which is vented to the ambient air via a needle valve (2204, KOFLOC, Japan) at a flow rate about 10 cm^3 min^{-1}. The 48-L aluminum cylinder for the working reference gas and the three 10-L aluminum cylinders for the standard gases are stored horizontally in thermally insulated boxes.

Custom software developed in LabVIEW (National Instruments Co., USA) and running on a PC controls valve operation and the acquisition of digital data from the O_2 and CO_2 analyzers and analog data from the mass flow and pressure sensors.

2.2 Cold trap

Among the constituents of tropospheric air, water vapor shows the widest range of variation, which causes apparent variations in the O_2 mole fraction of the air because the atmospheric O_2 is a major constituent of air (~21%). For example, a water vapor increase of 1 ppm causes a 0.2-ppm apparent decrease in the O_2 mole fraction. Therefore, a two-stage cold trap was adopted to reduce the water vapor in the sample air to less than 1 ppm. Figure 2a shows the first version of the cold trap, which consisted of a free-piston Stirling cooler (FPSC) module (SC-UE15R,

Twinbird, Japan), two disk-shaped aluminum blocks, a 1/8-inch SUS tube, and a drum-shaped glass vessel with a volume of about 1.0×10^3 cm^3. The aluminum blocks had four grooves for the 1/8-inch SUS tubes, including spare tubes to address clogging. And the aluminum blocks were placed between the cold head of the FPSC module and the glass vessel and contact was tight. A platinum resistance thermometer was inserted into the aluminum block, and a temperature controller (E5CC, OMRON, Japan) regulated the FPSC module to maintain the aluminum blocks at −80°C. The sample air was dried by passing through the glass vessel first and then the SUS tube.

When the first cold trap was used for preliminary measurements at NIES during the summer (with high humidity), it worked without clogging for at least 1 month, which is the typical duration for a round trip using the North American route. However, the measurements were often interrupted because the SUS tube and inlet of the glass vessel clogged when it was used aboard NC2, and the frequency of clogging increased as the season progressed from winter to spring to summer.

Thus, we changed the cold trap to the second design shown in Fig. 2b. In the second version of the cold trap, the cylindrical aluminum block with several holes is in contact with the cold head of the FPSC module, and a cylindrical glass vessel (volume of about 1.5×10^3 cm^3) and 1/8-inch SUS tube are inserted in the holes. The cold head and the aluminum block are insulated by a polyethylene resin cover. We began to use this cold trap for the shipboard measurements in September 2016, and the cold trap has not clogged since that time due to the more complete chilling of the glass vessel.

2.3 Calculation of ΔO_2, ΔCO_2, and $\delta(O_2/N_2)$

The O_2 analyzer, equipped with two fuel cell sensors, was designed to precisely measure the difference in the O_2 mole fraction between two air streams. Therefore, the change in the O_2 mole fraction of the sample gas is reported as a relative change with respect to the working reference gas, which is supplied from the high-pressure aluminum cylinder (48 L). In previous studies (e.g., Stephens et al., 2007; Thompson et al., 2007; van der Laan-Luijkx et al., 2010; Goto et al., 2013), the sample and reference air are alternately introduced into each fuel cell sensor by switching the 4-way 2-position valve at 1- to 5-min intervals. In this study, we adopted 2 min for the valve-switching intervals in light of the responses of the O_2 and CO_2 analyzer after valve switching, as described below. Figure 3a shows the temporal variation in the differential output signal of the O_2 analyzer during a test run in which a reference gas from a high-pressure cylinder was used as a sample gas. Although the flow rate in this system (10 cm^3 min^{-1}) is more than four times slower than the flow rates used in previous studies, the output signal shows an almost rectangular shape. The signal plateaus at least 1 min after the valve switching, and the output signal is

averaged from the second minute of the cycle (Fig. 3c). The deviation of the O_2 mole fraction in the sample gas from that of the working reference gas for the *i*-th 2-min interval, $\Delta O_{2,i}$, is computed based on the 1-min average according to the following equation:

$$\Delta O_{2,i} = (-1)^{(i-1)} [v_i - (v_{i-1} + v_{i+1})/2]/2 \quad (2)$$

where v_i represents the average of the output signal for the second minute of the *i*-th 2-min interval and the output signal represents the difference of the sample gas minus working reference gas when *i* is an odd number greater than 1.

In contrast to the O_2 analyzer, the CO_2 analyzer alternately measures the sample and working reference gases. The temporal variation of the output signal of the CO_2 analyzer is depicted in Figs. 3d and 3d. As shown in the figures, the output signal does not plateau until after more than 90 s because of the relatively low flow rate in comparison with the volume of the optical cell of the LI-840A analyzer (14.5 cm^3). Therefore, we compute an average of the output signal for the last 20 s of each 2-min interval. Then, the deviation of the CO_2 mole fraction of the sample gas from the working reference gas, $\Delta CO_{2,i}$, is computed according to

$$\Delta CO_{2,i} = (-1)^{(i-1)} [w_i - (w_{i-1} + w_{i+1})/2] \quad (3)$$

where w_i represents the average of the last 20 s of data for the *i*-th 2-min interval. Again, the sample gas is introduced into the CO_2 analyzer when *i* is an odd number greater than 1.

The variation in the atmospheric O_2 is expressed as the change in the $\delta(O_2/N_2)$ with respect to an arbitrary reference value, and the $\delta(O_2/N_2)$ is defined according to Eq. (1). Based on the ΔO_2 and ΔCO_2 values, $\delta(O_2/N_2)$ is given by the following equation:

$$\delta(O_2/N_2) = \frac{\Delta O_2}{S_{O_2}(1 - S_{O_2})} + \frac{\Delta CO_2}{(1 - S_{O_2})} \quad (4)$$

where S_{O2} represents the O_2 mole fraction in dry air (S_{O2} = 0.2094, Tohjima et al., 2005). In this calculation, we assume that only O_2 and CO_2 show more than ppm-level variation among all constituents of dry air, except nitrogen.

The time series of $\delta(O_2/N_2)$ and ΔCO_2 calculated by Eqs. (2), (3), and (4) for "sample" gas provided from a high-pressure cylinder against the working reference air are plotted in Fig. 4. The standard deviations for $\delta(O_2/N_2)$ and ΔCO_2 calculated from 20 h of data are 3.8 per meg and 0.1 ppm, respectively, which likely represents the best possible precision, because the measurements were taken in an air-conditioned laboratory.

2.4 Preliminary measurements of atmospheric O_2 and CO_2

We conducted preliminary observations of the atmospheric O_2 and CO_2 variations at Tsukuba, Japan, during the period July 10–17, 2015, to examine the performance of the O_2 and CO_2 measurement system. Outside air was drawn by the diaphragm pump from an air intake placed on top of our laboratory building. Two standard gases with high (−270 per meg) and low (−579 per meg) $\delta(O_2/N_2)$ values were repeatedly introduced into the O_2 analyzer for 32 min each at intervals of 25 h. We determined a single calibration line of linear response function for $\delta(O_2/N_2)$ values from all the measurements of the two standard gases during the observation. As for the CO_2 mole fraction, a single calibration line of linear function was determined from measurements of three standard gases with 387, 406, and 434 ppm only before the observation. The $\delta(O_2/N_2)$ value and CO_2 mole fraction were reported in our own original scales: NIES $\delta(O_2/N_2)$ scale (Tohjima et al., 2008) and the NIES 09 CO_2 scale (Machida et al., 2011).

As shown in Fig. 5, the observed $\delta(O_2/N_2)$ revealed a diurnal cycle with an increase in daytime and decrease at nighttime. This cycle was inversely correlated with the CO_2 mole fraction. A scatter plot of CO_2 and $\delta(O_2/N_2)$ shows a clear negative correlation with the $\Delta O_2/\Delta CO_2$ slope of −1.189±0.004, which is close to the land biotic O_2 to CO_2 exchange ratio of -1.10±0.05. Since the observation was conducted in summer and coal consumption is limited in Tsukuba, the $\Delta O_2/\Delta CO_2$ slope means that the observed CO_2 changes can be predominantly attributed to the activity on land. During the observation, 32-min measurements of a check gas (CPD-00012: −426 per meg for $\delta(O_2/N_2)$ and 407.12 ppm for CO_2) supplied from an aluminum 10-L cylinder were repeated twice daily. The $\delta(O_2/N_2)$ values and the CO_2 mole fractions of the check gas showed steady values (Fig. 5); the average and the standard deviation (±1σ) were −427.5±4.1 per meg for $\delta(O_2/N_2)$ and 407.11±0.11 ppm for CO_2. Moreover, there was no significant drift in the LI-840A analyzer during this observation. These results indicate the stability of the O_2 and CO_2 measurement system.

2.5 *In situ* measurements aboard NC2

In December 2015, the measurement system was installed in a deckhouse aboard NC2. An air intake was placed on a left-side deck rail of the navigation bridge, and air was drawn via a DK tube (NITTA, Japan) with an outer diameter of 10 mm and length of about 50 m. A 48-L aluminum cylinder for the working reference gas and three 10-L aluminum cylinders for the O_2 and CO_2 standard gases were placed in thermally insulated boxes, which were laid horizontally on a shelf to minimize the inhomogeneous distribution of $\delta(O_2/N_2)$ within the cylinders associated with temperature and pressure gradients (Keeling et al., 1998, 2007).

The two standard gases with −579 per meg (tank #CPD-00010) and −270 per meg (tank #CPD-00011) were used for calibration of the O_2 analyzer. Since the CO_2 mole fraction of these two standard gases are almost same (~407 ppm), we additionally used a third standard gas with a CO_2 mole fraction of 448.3 ppm (tank #CPB-17350) to calibrate the CO_2 analyzer. During every 24 h period, these three standard gases were measured for 32 min each. To determine the calibration lines for both the O_2 and CO_2 analyzers precisely, the measurements of the three standard gases were repeated over 24 h when NC2 berthed at the port of Tahara, Japan.

3 Results and discussion

3.1 Influence of ship motion

After beginning the *in situ* measurements aboard NC2, we found that the ship motions did not affect the response of the CO_2 analyzer but did seriously affect the response of the O_2 analyzer. Figures 6a and 6b show temporal variations in the output signal of the O_2 analyzer for the standard gas when NC2 was berthed at the port of Tahara and was cruising on the Pacific Ocean, respectively. The output signal during the cruise (Figs. 6b and 6d) shows apparent variations with peak-to-peak amplitudes of more than several tens of ppm and peak-to-peak periods of about 20 s. Pickers (2016) reported that similar apparent variations caused by ship motion were superimposed on output signals of individual fuel cells in an Oxzilla-II analyzer. However, in Pickers' instrument, the differential signal of both fuel cells did not show apparent variations because the motion-induced variations were almost compensated completely by the differential signals.

We installed a 3-dimensional accelerometer on the O_2 analyzer on March 3, 2016, to examine the relationship between the Oxzilla output signals and the ship's motion. The apparent variations in the output signal were associated with the variations in the acceleration of one axis or another and both amplitudes were roughly proportional to each other. However, we have not succeeded in describing the apparent variations with a linear function of the measured accelerations. This is because the sensitivity of the O_2 analyzer to the acceleration along the three axes seems to be unstable with time. Therefore, at this stage we cannot remove the apparent variations associated with the ship motions with a simple algorithm.

Figure 7 shows temporal variations in the $\delta(O_2/N_2)$ value of the two standard gases relative to the working gas during the 1-yr period of this study. In the figure, each blue circle represents the 32-min average of the standard gas during the voyages. The standard deviations of the 32-min averages were less than 13 per meg, suggesting that

the averaging procedure for several tens of minutes can effectively suppress the errors caused by ship motion. For example, the expected standard deviation of the hourly $\delta(O_2/N_2)$ value for the standard gases is 9 per meg ($=13/2^{1/2}$).

The uncertainties of the 32-min averages of the standard gases are too large for calibration of the O_2 analyzer. In Fig. 7, the average $\delta(O_2/N_2)$ values of the standard gases determined when NC2 was berthed at the port of Tahara are also plotted as black circles with error bars showing the standard deviations. Unfortunately, the standard deviations for the standard gases were larger than the expected values obtained in our laboratory, as discussed in Section 2.3. However, the standard errors were lower than 2 per meg because the measurements were continued for more than 5 h for the individual standard gases. Therefore, we calibrated the O_2 analyzer using calibration lines based on the results at the port just before and after each round-trip voyage.

3.2 Comparison between flask sampling and *in situ* observations

During the 1-yr period from December 2015 through November 2016, the *in situ* measurements of the atmospheric O_2 and CO_2 were conducted during nine round-trip voyages, from NC2-123 to NC2-131, along the North American route. The individual cruise tracks are depicted in Fig. 8a, where thin lines correspond to intervals of missing measurements. We obtained no *in situ* data during the two westbound voyages of NC2-123 and NC2-128 because the cold trap became clogged. Along with the *in situ* measurements, air samples were collected in seven 2.5-L glass flasks at fixed longitudes (130°W, 145°W, 160°W, 175°W, 170°E, 155°E, and 145°E) during each westbound cruise.

The time series of $\delta(O_2/N_2)$, CO_2, and APO data taken from the *in situ* measurements and the flask samplings are shown in Fig. 9. The APO is computed based on the $\delta(O_2/N_2)$ and CO_2 mole fraction in accordance with the following equation:

$$\delta APO = \delta(O_2/N_2) + 1.1 \times \frac{X_{CO_2}}{S_{O_2}} - 1850 \quad (5)$$

where 1850 is an arbitrary APO reference point adopted by NIES. In Fig. 9, each point for the *in situ* measurement represents the hourly average and the data outside the longitudinal range between 140°E and 128°W are excluded because of significant contamination by anthropogenic emissions from the coastal regions of both Japan and North America. The time series in Fig. 9 clearly shows seasonal cycles and the *in situ* data seem to agree with the flask data. The differences in the $\delta(O_2/N_2)$, CO_2, and APO values between the *in situ* and the 39 flask measurements (*in situ* – flask) are depicted in Fig. 10. The averaged differences with standard deviations were −2.8±9.4 per meg of

$\delta(O_2/N_2)$, −0.02±0.33 ppm of CO_2, and −2.9±9.5 per meg of APO. Taking into account the uncertainties of the flask measurements (5 per meg for $\delta(O_2/N_2)$ and 0.05 ppm for CO_2 measurements, Tohjima et al., 2003), we conclude that the uncertainties of the *in situ* measurements aboard NC2 were 8.0 per meg for $\delta(O_2/N_2)$ and 0.33 ppm for CO_2. The differences between flask sampling and *in situ* measurements by the GC/TCD method were reported as −0.6±9.1 per meg of APO on the Oceanian route (Tohjima et al., 2015), and 7.0±9.9 per meg of $\delta(O_2/N_2)$ at Cape Ochi-ishi (Yamagishi et al., 2008). From these results, we conclude that the reliability of the O_2 measurements of this study is similar to that of the GC/TCD method.

The time series of the *in situ* data shown in Fig. 9 do not necessarily show smooth changes, which may be partly attributed to the fact that the aboard observations were conducted in the broad area of the North Pacific. For example, the APO values show relatively low values (< −180 per meg) during the eastbound voyage NC2-125 in early March and high values (> −100 per meg) during the eastbound voyage NC2-127 in late May. The longitudinal distributions of the 5-h running average of APO for the individual round-trip cruises are depicted in Fig. 8b, which clearly shows these anomalously low (blue line of NC2-125) and high (light blue line of NC2-127) APO distributions. Preliminary analyses of the cause of these anomalies points to atmospheric transport and the expected air-sea gas exchanges in the source regions. Detailed discussions of the anomalous changes are beyond the scope of this paper and will be presented in a future publication.

3.3 Distribution of seasonal cycles in the North Pacific

We investigated the longitudinal distribution of the seasonal amplitude of APO in the middle latitudes of the North Pacific using the 1 yr of *in situ* data within the area of 29°N–45°N and 140°E–130°W (Fig. 8a). The *in situ* data were binned into 10 longitudinal bands (140°E–150°E, 150°E–160°E, …, 140°W–130°W) and fitted to the following function using a least-squares method:

$$f(t) = a_0 + a_1 t + \sum_{i=1}^{2} [a_{2i} \sin(2\pi i t) + a_{2i+1} \cos(2\pi i t)] \quad (6)$$

where a_1 is a detrending coefficient (−7.9 per meg yr^{-1}) determined from the APO values measured from the flask samples collected aboard NC2 during the 2-yr period 2014–2016.

The detrended *in situ* data for the individual longitudinal bins and the fitted average seasonal cycles are shown in Fig. 11. The APO seasonal amplitudes for the 10 bins are plotted along with the longitude in Fig. 12a. For comparison, we also plot seasonal amplitudes of APO in the North Pacific reported by Tohjima et al. (2012). In the

previous study, APO data from the flask samples collected in the Pacific during the period from 2002 to 2008 were binned into several rectangular regions and the seasonal cycles for the binned data were examined in the same way as in this study. The seasonal amplitudes in the previous study varied from 20 per meg to 110 per meg, while those in this study varied from 51 per meg to 73 per meg. The difference in the seasonal amplitudes seems to be explained by the dependence of the latitudinal distribution, which is clearly shown in Fig. 12b, where all the seasonal amplitudes shown in Fig. 12a are plotted along with the latitude. Such latitudinal dependence of the APO amplitude was previously pointed out for data from the western Pacific (Tohjima et al., 2005, 2012). On the other hand, this study reveals that the longitudinal variability in the seasonal amplitude of APO in the North Pacific is rather small. This preliminary analysis suggests that the temporally and spatially dense atmospheric O_2 and CO_2 data obtained from the *in situ* observation aboard NC2 will enhance our understanding of air-sea gas exchange in the North Pacific.

4 Conclusion

We developed a ship-borne system to continuously measure atmospheric O_2 and CO_2 variations based on a fuel cell oxygen analyzer (Oxzilla-II) and a non-dispersive infrared CO_2 analyzer (LI-840A). To reduce the consumption rate of working reference gas and standard gases supplied from high-pressure cylinders, a relatively low flow rate of 10 cm^3 min^{-1} was adopted for the measurement system. By keeping the flow rate and pressure of the system constant, we achieved precisions of 3.8 per meg for the O_2 measurements and 0.1 ppm for the CO_2 measurements in the laboratory.

We installed the measurement system on commercial cargo ship NC2 and started aboard continuous measurements in December 2015. We found that the ship motion significantly affected the output signal of the O_2 analyzer; apparent wavy variations with amplitudes of more than 20 ppm and peak-to-peak periods of about 20 s were superimposed on the output signals during the voyage. Although this variation has not been eliminated yet, 1-h averaging considerably suppresses the variation associated with the ship motion because of the oscillatory nature of the apparent variations. From the comparison between the *in situ* measurements and simultaneously collected flask samples, we concluded that the uncertainties of $\delta(O_2/N_2)$ and CO_2 mole fraction for the *in situ* measurements are about 9 per meg and about 0.3 ppm, respectively.

Using the *in situ* data obtained during the 1-yr period from December 2015 to November 2016, we examined longitudinal (140°E–130°W) distribution of seasonal APO amplitude at the middle latitudes (29°N–45°N) in the

North Pacific. The amplitudes showed rather small longitudinal variability, with a range from 51 per meg to 73 per meg in comparison to the latitudinal variations reported by Tohjima et al. (2012). Although the problem related to motion-induced degradation of O_2 measurement precision has not been resolved, this study clearly demonstrated that *in situ* observation aboard cargo ships can extend the coverage of the atmospheric O_2 and CO_2 data to a degree that flask sampling could never achieve.

Acknowledgment

We gratefully acknowledge the generous cooperation of Toyofuji Shipping Co. and Kagoshima Senpaku Co. for providing us the opportunity to make the aboard atmospheric observations. Thanks are also expressed to the crew of *New Century 2*. We would like to thank Tomoyasu Yamada, Nobukazu Oda, and other members of the Global Environmental Forum for their continued support in maintaining the O_2 and CO_2 measurement system. We thank Hisayo Sandanbata, Eri Matsuura, and Motoki Sasakawa of the NIES for their continued support in the O_2 and CO_2 analysis of flask samples. This work was financially supported by a Grant-in-Aid for Scientific Research, and in part by the Global Environmental Research Coordination System, from the Ministry of the Environment, Japan (E1451).

References

Battle, M., Bender, M. L., Tans, P. P., White, J. W. C., Ellis, J. T., Conway, T., and Francey, R. J.: Global carbon sinks and their variability inferred from atmospheric O_2 and $\delta^{13}C$, Science, 287, 2467–2470, doi:10.1126/science.287.5462.2467, 2000.

Battle, M., Fletcher, S. M., Bender, M. L., Keeling, R. F., Manning, A. C., Gruber, N., Tnas, P. P., Hendricks, M. B., Ho, D. T., Simonds, C., Mika, R., and Paplawsky, B.: Atmospheric potential oxygen: New observations and their implications for some atmospheric and oceanic models, Global Biogeochem. Cycles, 20, GB1010, doi:10.1029/2005GB002534, 2006.

Balkanski, Y., Monfray, P., Battle, M., and Heimann, M.: Ocean primary production derived from satellite data: an evaluation with atmospheric oxygen measurements. Glob. Biogeochem. Cycles. 13, 257–271, 1999.

Bender, M. L., Tans, P. P., Ellis, J. T., Orchardo, J. and Habfast, K.: A high precision isotope ratio mass spectrometry method for measuring the O_2/N_2 ratio of air, Geochim. Cosmochim. Acta, 58, 4751–4758, 1994.

Bopp, L., Le Quere, C., Heimann, M., Manning, A. C. and Monfray, P.: Climate-induced oceanic oxygen fluxes: Implications for the contemporary carbon budget, Global Biogeochem. Cycles, 16, 1022, doi:10.1029/2001GB001445, 2002.

Goto, D., Morimoto, S., Ishidoya, S., Ogi, A., Aoki, S., and Nakazawa, T.: Development of a High Precision Continuous Measurement System for the Atmospheric O_2/N_2 Ratio and Its Application at Aobayama, Sendai, Japan, J. Meteorol. Soc. Japan, 91, 179–192, doi:10.2151/jmsj.2013-206, 2013.

Ishidoya, S., Morimoto, S., Aoki, S., Taguchi, S., Goto, D., Murayama, S., and Nakazawa, T.: Oceanic and terrestrial biospheric CO_2 uptake estimated from atmospheric potential oxygen observed at Ny-Ålesund, Svalbard, and Syowa, Antarctica, Tellus B, 64, 18924, doi:10.3402/tellusb.v6i0.18924, 2012.

Keeling, R. F.: Development of an interferometric oxygen analyzer for precise measurement of the atmospheric O_2 mole fraction, Ph.D. thesis, Harvard Univ., Cambridge, U.S.A., 178 pp., 1988.

Keeling, R. F. and Garcia, H. E.: The change in oceanic O_2 inventory associated with recent global warming, Proc. Natl. Acad. Sci. U. S. A., 99, 7848–7853, doi:10.1073/pnas.122154899, 2002.

Keeling, R. F. and Shertz, S. R.: Seasonal and interannual variations in atmospheric oxygen and implications for the global carbon cycle, Nature, 358, 723–727, 1992.

Keeling, R. F., Najjar, R. P., Bender, M. L. and Tans, P. P.: What atmospheric oxygen measurements can tell us about the global carbon cycle, Global Biogeochem. Cycles, 7, 37–67, 1993.

Keeling, R. F., Manning, A. C., McEvoy, E. M. and Shertz, S. R.: Methods for measuring changes in atmospheric O_2 concentration and their application in southern hemisphere air, J. Geophys. Res. 103, 3381–3397, 1998.

Keeling, R. F., and Manning, A. C.: Studies of recent changes in atmospheric O_2 content, Treatise on Geochemistry: Second Edition, UNSPECIFIED, pp. 385–404, ISBN9780080983004, 2014.

Keeling, R. F., Manning, A. C., Paplawsky, W. J., and Cox, A. C.: On the long-term stability of reference gases for atmospheric O_2/N_2 and CO_2 measurements, Tellus B, 59, 3–14, doi:10.1111/j.1600-0889.2006.00228x, 2007.

Lueker, T. J., Walker, S. J., Vollmer, M. K., Keeling, R. F., Nevison, C. D., and Weiss, F.: Coastal upwelling air-sea fluxes revealed in atmospheric observations of O_2/N_2, CO_2 and N_2O, Geophys. Res. Lett., 30, 1292, doi:10.1029/2002GL016615, 2003.

Machida, T., Tohjima, Y., Katsumata, K. and Mukai, H.: A new CO_2 calibration scale based on gravimetric one-step dilution cylinders in National Institute for Environmental Studies-NIES 09 CO_2 scale, In: Report of the 15thWMO Meeting of Experts on Carbon Dioxide Concentration and Related Tracer Measurement Techniques (ed. W. A. Brand), Jena, Germany, September 7–10, 2009, WMO/GAW Report No. 194, WMO, Geneva, Switzerland, pp. 114–118, 2011.

Manning, A. C., Keeling, R. F. and Severinghaus, J. P.: Precise atmospheric oxygen measurements with a paramagnetic oxygen analyzer, Global Biogeochem. Cycle, 13, 1107–1115, 1999.

Manning, A. C. and Keeling R. F.: Global oceanic and biotic carbon sinks from the Scripps atmospheric oxygen flask sampling network, Tellus B, 58, 95–116, doi:10.1111/j.1600-0889.2006.00175.x, 2006.

Naegler, T., Ciais, P., Orr, J. C., Aumont, O., and Rodenbeck, C.: On evaluating ocean models with atmospheric potential oxygen, Tellus B, 59, 138–156, doi:10.1111/j.1600-0889.2006.00197.x, 2007.

Nevison, C. D., Mahowald, N. M., Doney, S. C., Lima, I. D., and Cassar, N.: Impact of variable air-sea O_2 and CO_2 fluxes on atmospheric potential oxygen (APO) and land-ocean carbon sink partitioning, Biogeosciences, 5, 875–889, doi:10.5194/bg-5-875-2008, 2008.

Nevison, C. D., Keeling, R. F., Kahru, M., Manizza, M., Mitchell, B. G., and Cassar, N.: Estimating net community production in the Southern Ocean based on atmospheric potential oxygen and satellite ocean color data, Global Biogeochem. Cycle, 26, GB1020, doi:10.1029/2011GB004040, 2012.

Nevison, C. D., Manizza, M., Keeling, R. F., Kahru, M., Bopp, L., Dunne, J., Tiputra, J., Ilyina, T., and Mitchell, B. G.: Evaluating the ocean biogeochemical components of Earth system models using atmospheric potential oxygen and ocean color data, Biogeosciences, 12, 193–208, doi:10.5194/bg-12-193-2015, 2015.

Nevison, C. D., Manizza, M., Keeling, R. F., Stephens, B. B., Bent, J. D., Dunne, J., Ilyina, T., Long, M., Reslandy, L., Tjiputra, J., and Yukimoto, S.: Evaluating CMIP ocean biogeochemistry and Southern Ocean carbon uptake using atmospheric potential oxygen: Present-day performance and future projection, Geohys. Res. Lett., 43, 2077–2085, doi:10.1002/2015GL067584, 2016.

Plattner, G. K., Joos, F. and Stocker, T. F.: Revision of the global carbon budget due to changing air-sea oxygen fluxes, Global Biogeochem. Cycles, 16, 1096, doi:10.1029/2001GB001746, 2002.

Pickers, P.: New applications of continuous atmospheric O_2 measurements: meridional transects across the Atlantic Ocean, and improved quantification of fossil fuel-derived CO_2, Ph.D. thesis, University of East Anglia, England, 262 pp., 2016.

Pickers, P. A., Manning, A. C., Sturges, W. T., Le Quéré, C., Mikaloff Fletcher, S. E., Wilson, P. A., and Etchells, A. J.: In situ measurements of atmospheric O_2 and CO_2 reveal an unexpected O_2 signal over the tropical Atlantic Ocean, Global Biogeochem. Cycles, 31, 1289–1305, doi:10.1002/2017GV005631, 2017.

Severinghaus, J. P.: Studies of the terrestrial O_2 and carbon cycles in sand dune gases and in Biosphere 2, Ph.D. thesis, Columbia Univ., New York, U.S.A., 148 pp., 1995.

Stephens, B. B., Keeling, R. F., Heimann, M., Six, K. D., Murnane, R. and Caldeira, K.: Testing global ocean carbon cycle models using measurements of atmospheric O_2 and CO_2 concentration, Global Biogeochem. Cycles, 12, 213–230, 1998.

Stephens, B. B., Keeling, R. F. and Paplawsky, W.: Shipboard measurements of atmospheric oxygen using a vacuum-ultraviolet absorption technique, Tellus B, 55, 857–878, doi:10.1046/j.1435-6935.2003.00075.x, 2003.

Stephens, B. B., Bakwin, P. S., Tans, P. P., Teclaw, R. M. and Baumann, D. D.: Application of a differential fuel-cell analyzer for measuring atmospheric oxygen variations, J. Atmos. Ocean Tech., 24, 82–94, doi:10.1175/JTECH1959.1, 2007.

Thompson, R. L., Manning, A. C., Lowe, D. C. and Weatherburn, D. C.: A ship-based methodology for high precision atmospheric oxygen measurements and its application in the Southern Ocean region, Tellus B, 59,643–653, doi:10.1111/j.1600-0889.2007.00292.x, 2007.

Tohjima, Y.: Method for measuring changes in the atmospheric O_2/N_2 ratio by a gas chromatograph equipped with a thermal conductivity detector, J. Geophys. Res., 105, 14575–14584, doi:10.1029/2000JD900057, 2000.

Tohjima, Y., Mukai, H., Machida, T., and Nojiri, Y.: Gas-chromatographic measurements of the atmospheric oxygen/nitrogen ratio at Hateruma Island and Cape Ochi-ishi, Japan, Geophys. Res. Lett., 30, 1653, doi:10.1029/2003GL017282, 2003.

Tohjima, Y., Machida, T., Watai, T., Akama, I., Amari, T. and Moriwaki, Y.: Preparation of gravimetric standards for measurements of atmospheric oxygen and reevaluation of atmospheric oxygen concentration, J. Geophys. Res., 110, D11302, doi:10.1029/2004JD005595, 2005.

Tohjima, Y., Mukai, H., Nojiri, Y., Yamagishi, H., and Machida, T.: Atmospheric O_2/N_2 measurements at two Japanese sites: Estimation of global oceanic and land biotic carbon sinks and analysis of the variations in atmospheric potential oxygen (APO), Tellus B, 60, 213–225, doi:10.1111/j.1600-0889.2007.00334.x, 2008.

Tohjima, Y., Minejima, C., Mukai, H., Machida, T., Yamagishi, H., and Nojiri, Y.: Analysis of seasonality and annual mean distribution of atmospheric potential oxygen (APO) in the Pacific region, Global Biogeochem. Cycles, 26, GB4008, doi:10.1029/2011GB004110, 2012.

Tohjima, Y., Terao, Y., Mukai, H., Machida, T., Nojiri, Y., and Maksyutov, S.: ENSO-related variability in latitudinal distribution of annual mean atmospheric potential oxygen (APO) in the equatorial Western Pacific, Tellus B, 67, 1–15, doi:10.3402/tellusb.v67.25869, 2015.

van der Laan-Luijkx, I. T., Neubert, R. E. M., van der Laan, S., and Meijer, H. A. J.: Continuous measurements of atmospheric oxygen and carbon dioxide on a North Sea gas platform, Atmos. Meas. Tech., 3, 113–125, doi:10.5194/amt-3-113-2010, 2010.

Yamagishi, H., Tohjima, Y., Mukai, H., and Sasaoka, K.: Detection of regional scale sea-to-air oxygen emission related to spring bloom near Japan by using in-situ measurements of the atmospheric oxygen/nitrogen ratio, Atmos. Chem. Phys., 8, 3325–3335, doi:10.5194/acp-8-3325-2008, 2008.

Yamagishi, H., Tohjima, Y., Mukai, H., Nojiri, Y., Miyazaki, C., and Katsumata, K.: Observation of atmospheric oxygen/nitrogen ratio aboard a cargo ship using gas chromatography/thermal conductivity detector, J. Geophys. Res., 117, D04309, doi:10.1029/2011JD016939, 2012.

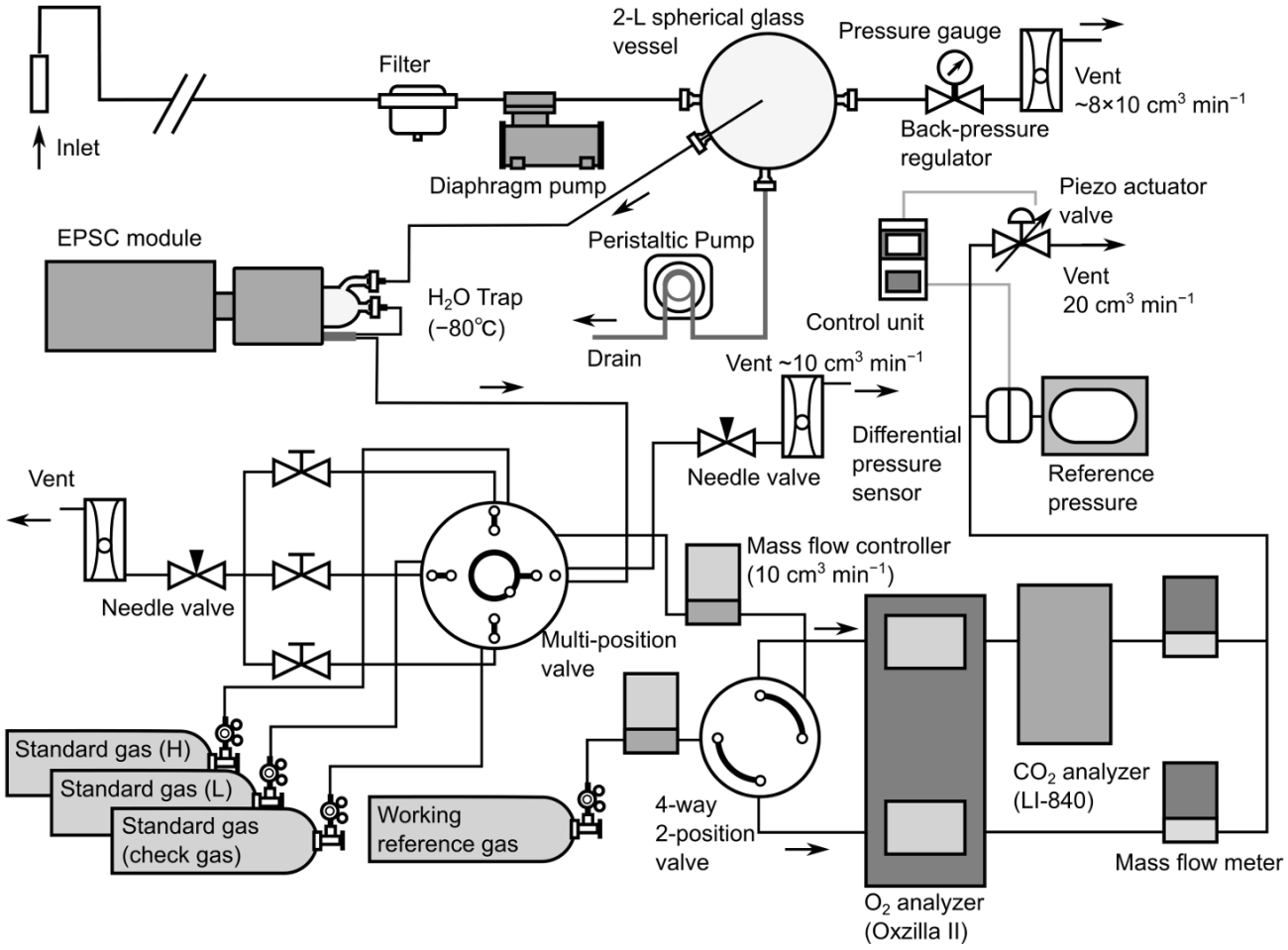

Figure 1: Schematic diagram of atmospheric O_2 and CO_2 measurement system used aboard cargo ship NC2.

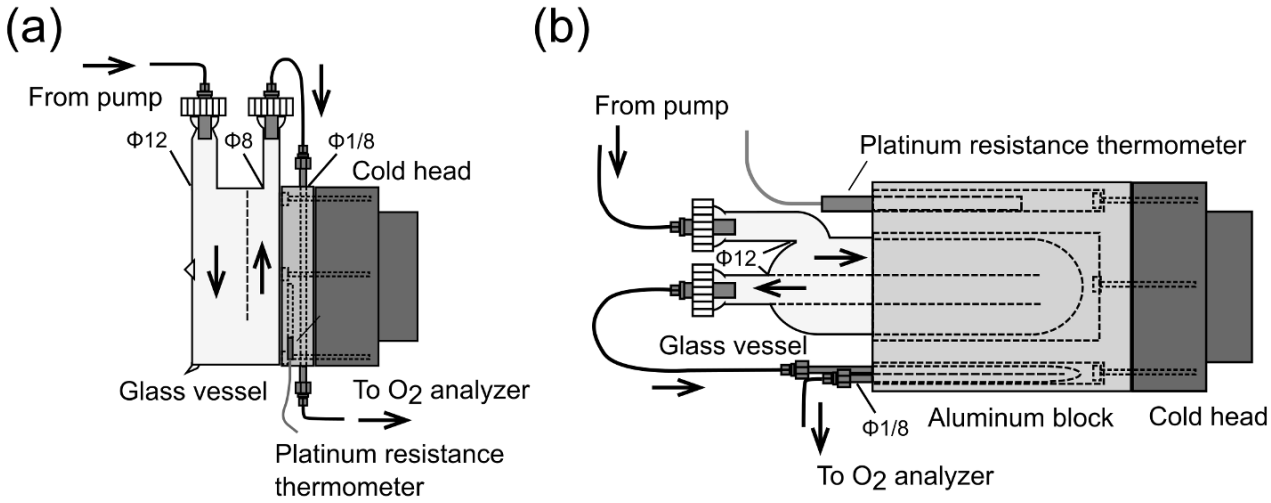

Figure 2: Schematic diagram of (a) first and (b) second versions of cold trap for reducing water vapor in samples.

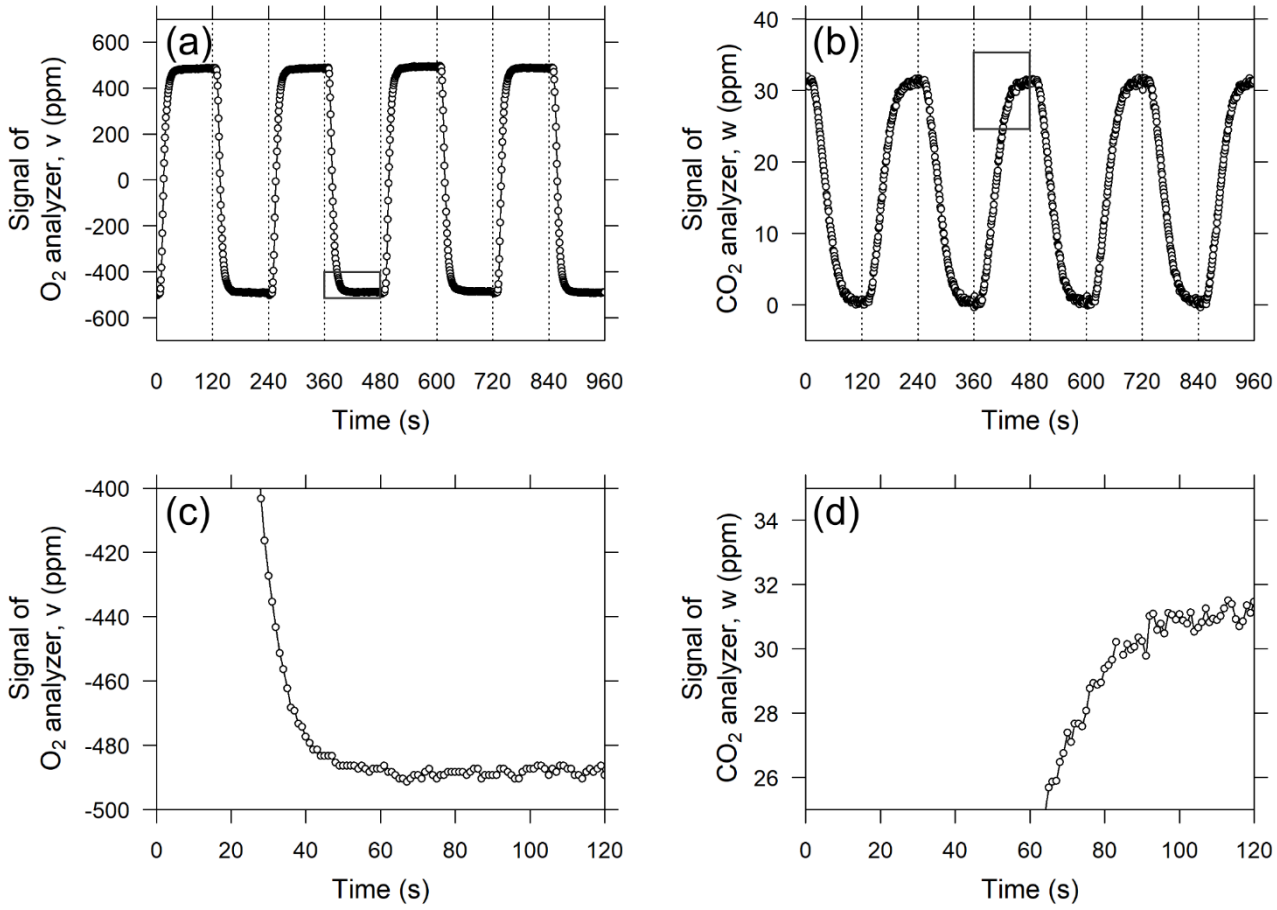

Figure 3: Temporal variations in the output signals of (a) O_2 analyzer and (b) CO_2 analyzer when standard air from a high-pressure cylinder was measured as sample air. The vertical dashed lines denote the timing of valve switching. Panels (c) and (d) are closeups of areas marked with rectangles in panels (a) and (b), respectively, and the horizontal axis shows the time from valve switching.

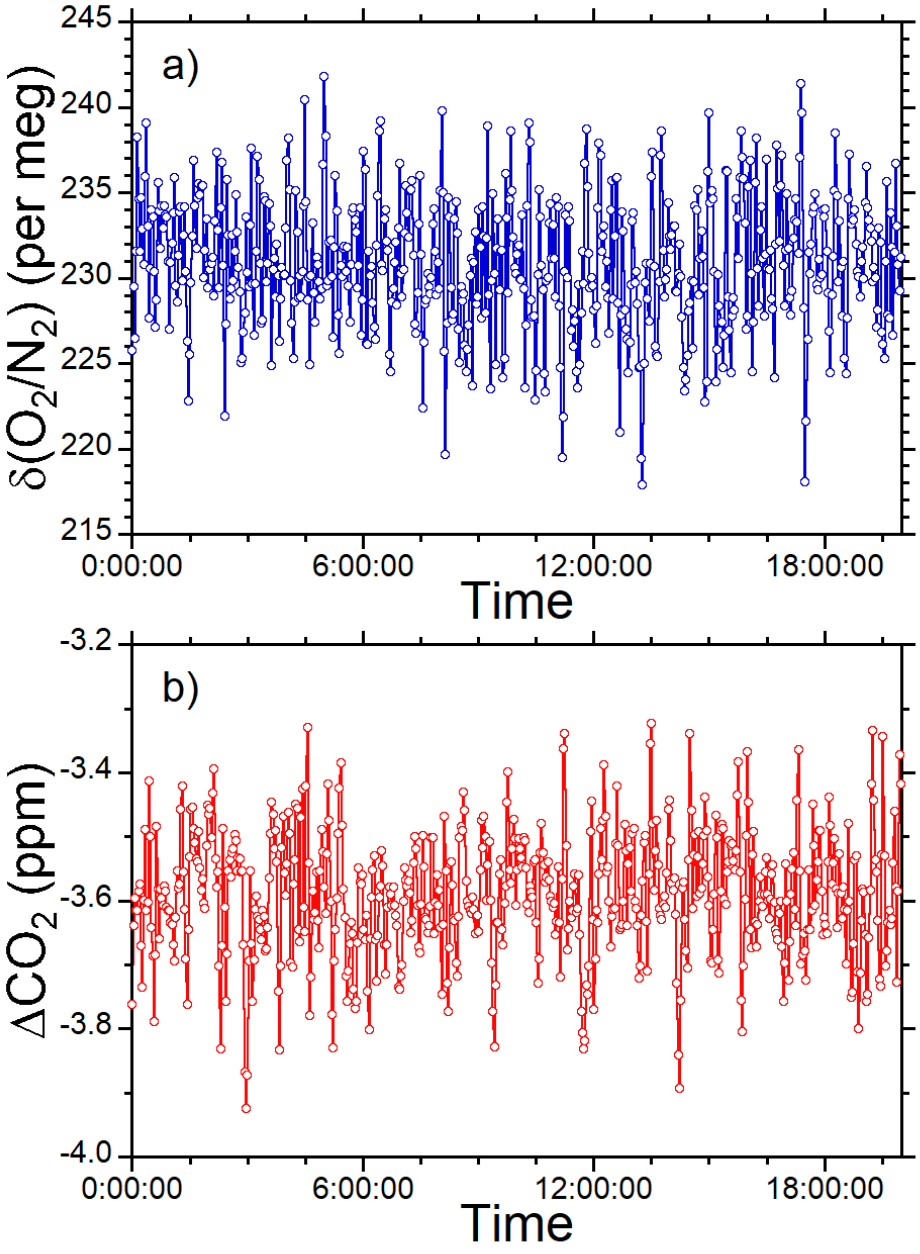

Figure 4: Time series of $\delta(O_2/N_2)$ and ΔCO_2 calculated by Eqs. (2), (3), and (4) for sample air provided from high-pressure cylinder against the working reference.

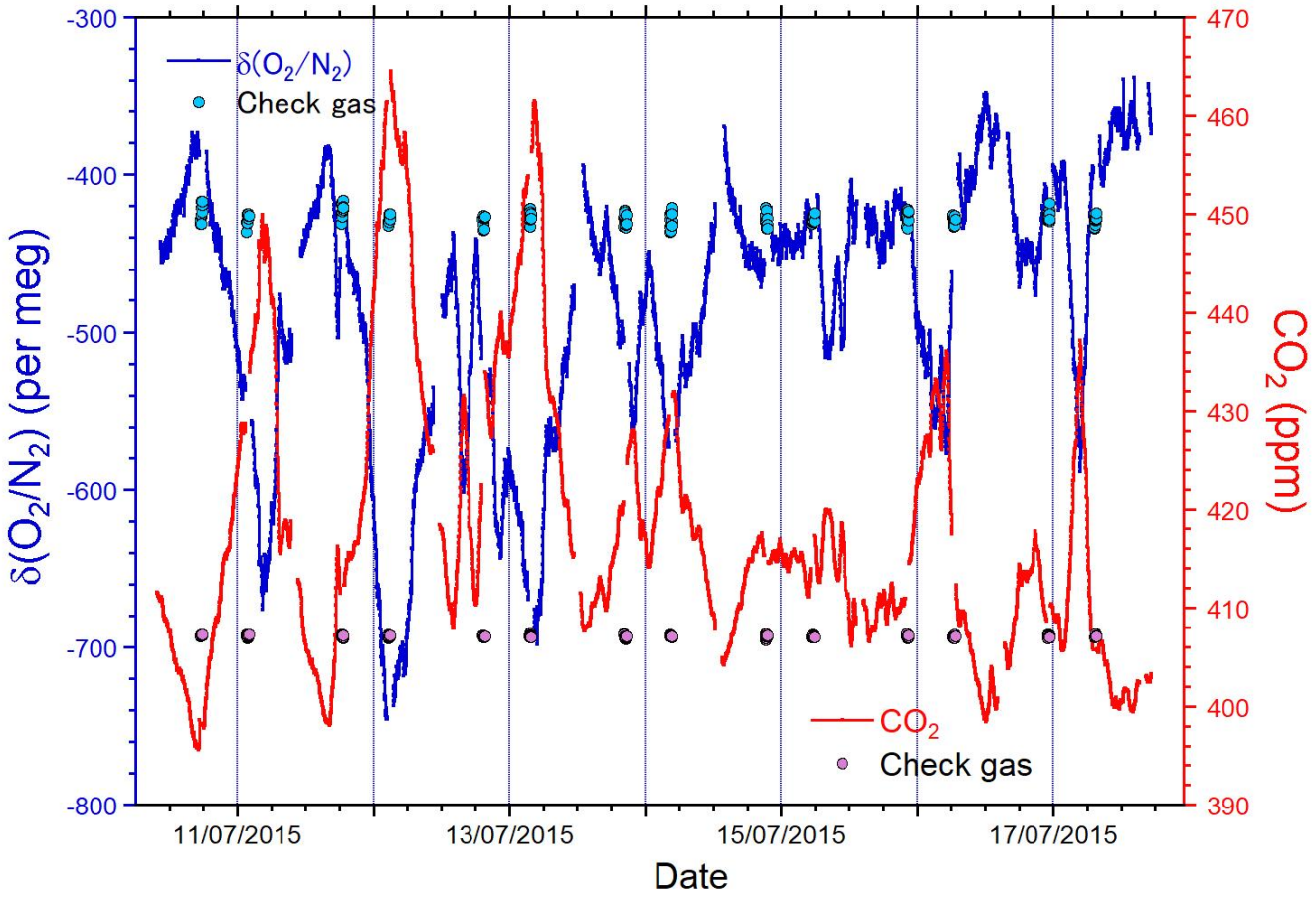

Figure 5: Time series of $\delta(O_2/N_2)$ (blue, left axis) and CO_2 mole fraction (red, right axis) observed at Tsukuba during July 10–17, 2015. The $\delta(O_2/N_2)$ and CO_2 mole fraction of the periodically measured check gas are also depicted as light blue and pink circles, respectively.

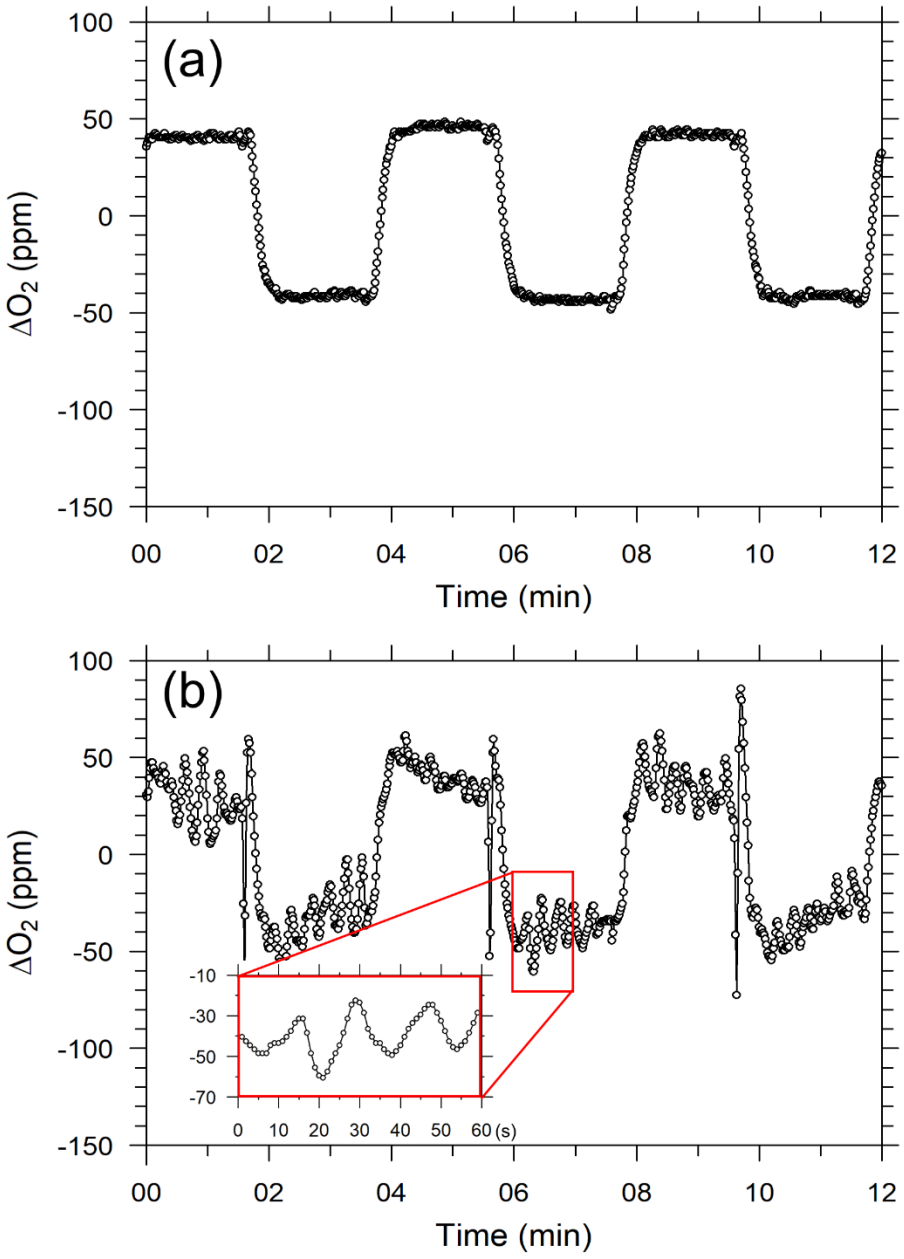

Figure 6: Temporal variations in differential output signals of O_2 analyzer for six measurement cycles of O_2 standard gas while ship was (a) in harbor and (b) cruising.

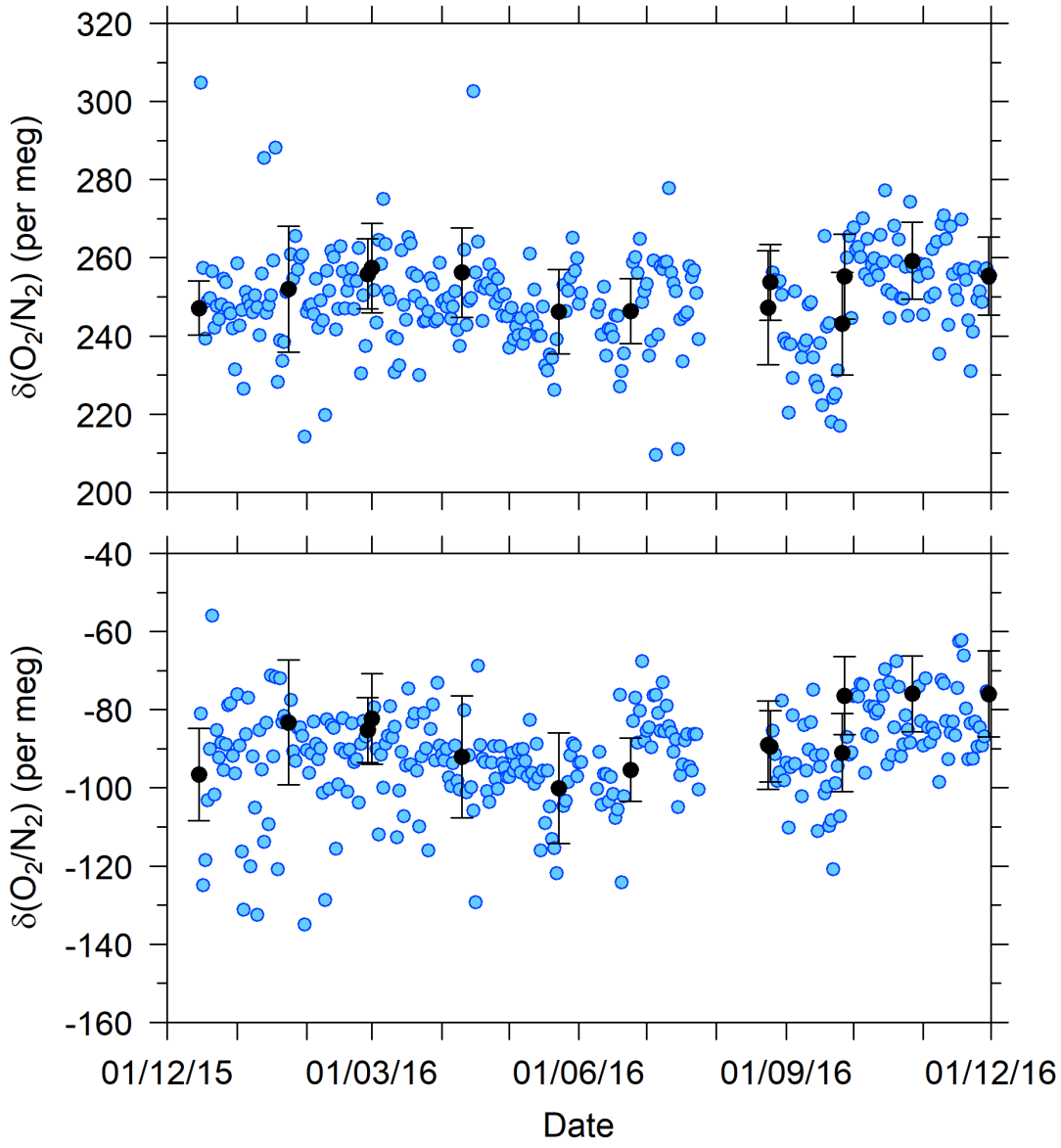

Figure 7: Time series of differences in $\delta(O_2/N_2)$ for two standard gases (top) CPD-00011 and (bottom) CPD-00010 with respect to working reference gas, as determined aboard NC2 during the 1-yr period of this study. Blue circles represent 32-min average values of standard gas measurements carried out at 24-h intervals. Black circles represent the averages of calibrations conducted when NC2 was berthed at the port of Tahara, and the error bars represent standard deviations.

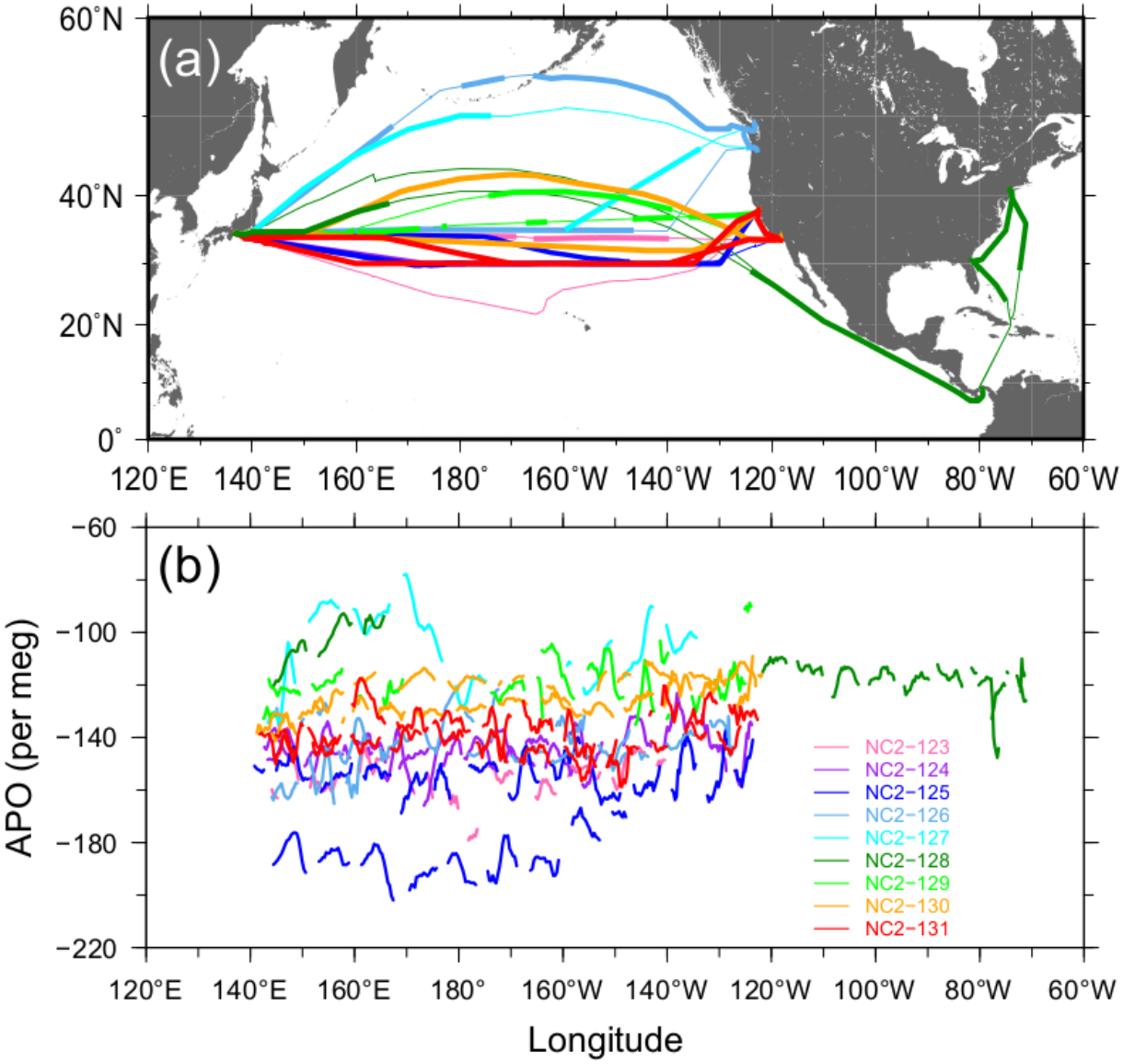

Figure 8: (a) Cruise tracks of NC2 for nine round trips (NC2-123, NC2-124, …, NC2-131) during the period from December 2015 to November 2016. Thin lines represent intervals where *in situ* measurements aboard NC2 were interrupted. (b) Longitudinal distribution of hourly APO taken from the nine cruises. Five-hour running averages are applied to the hourly data to reduce signal noise.

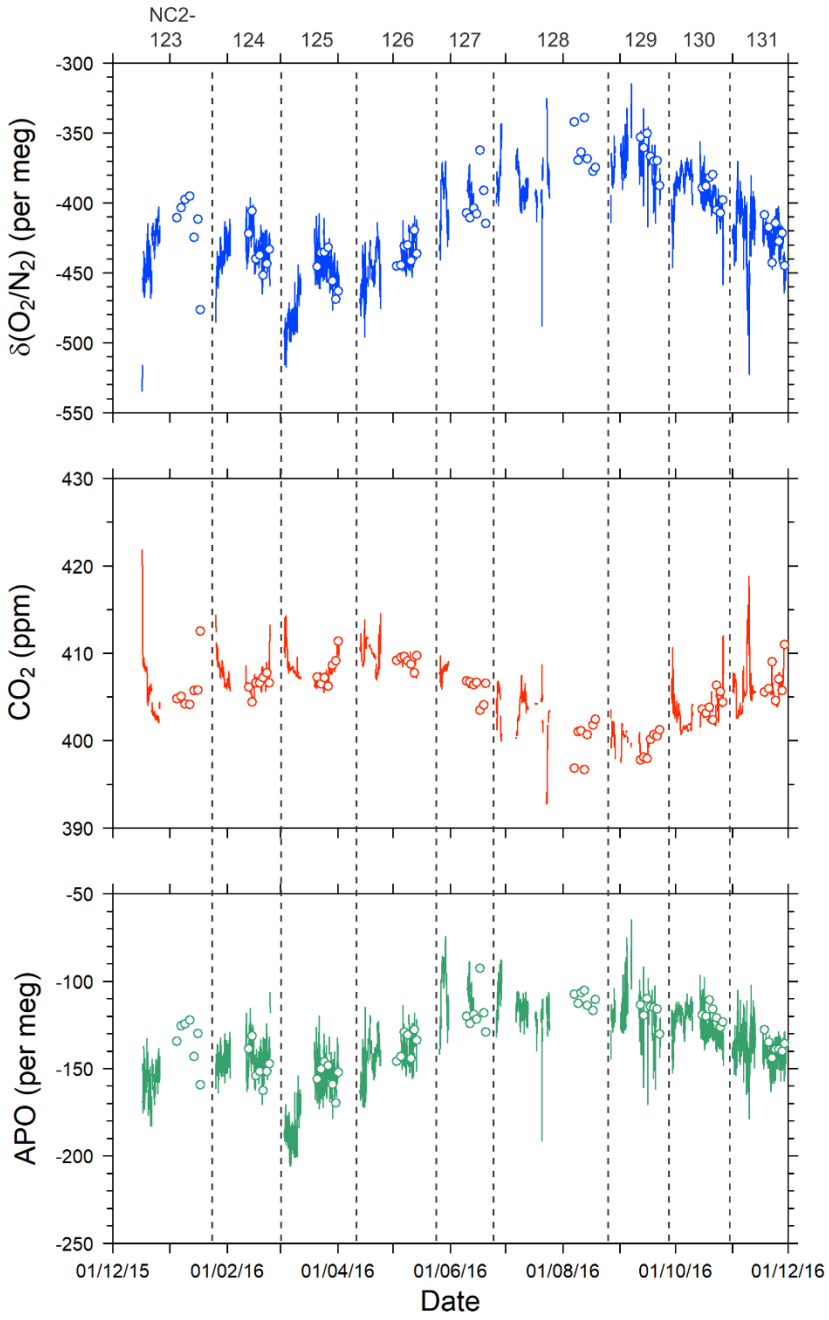

Figure 9: Time series of (top) $\delta(O_2/N_2)$, (middle) CO_2, and (bottom) APO during 1-yr period from December 2015 to November 2016. Lines indicate continuous observation, and circles indicate flask measurements. Data obtained near the coasts of Japan and North America are excluded. Vertical dashed lines separate each cruise and the top labels represent cruise numbers.

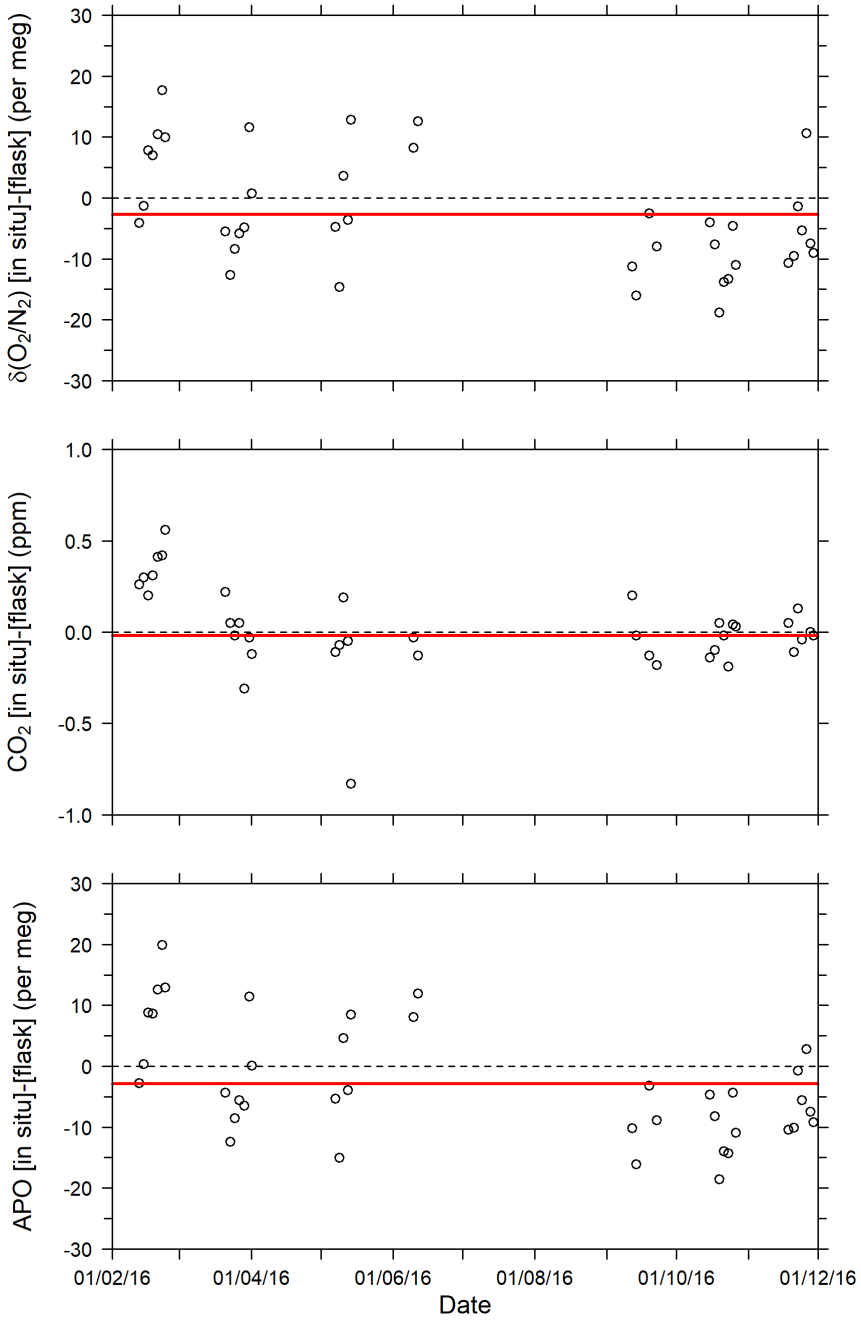

Figure 10: Time series of differences of (top) $\delta(O_2/N_2)$, (middle) CO_2, and (bottom) APO between the *in situ* measurements and flask measurements (*in situ* – flask). The red lines show average values.

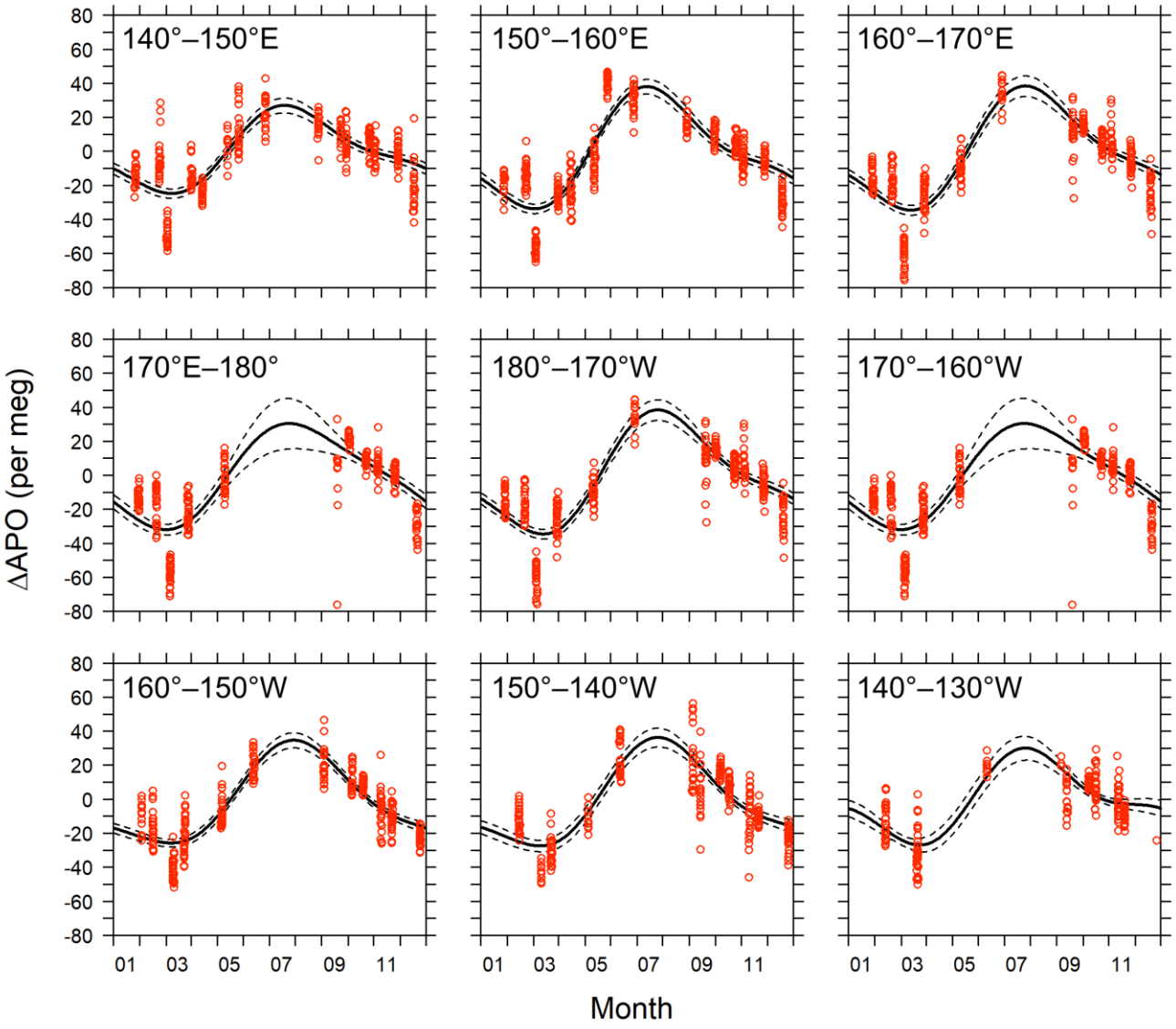

Figure 11: Detrended seasonal variations of APO for the 10 longitudinal bins within the rectangular area of 29°N–45°N and 140°E–130°W. Red circles represent hourly averages of *in situ* APO data. Solid lines are average seasonal cycles determined by a least-squares method. Dashed lines indicate 95% confidence intervals determined by a linear prediction model.

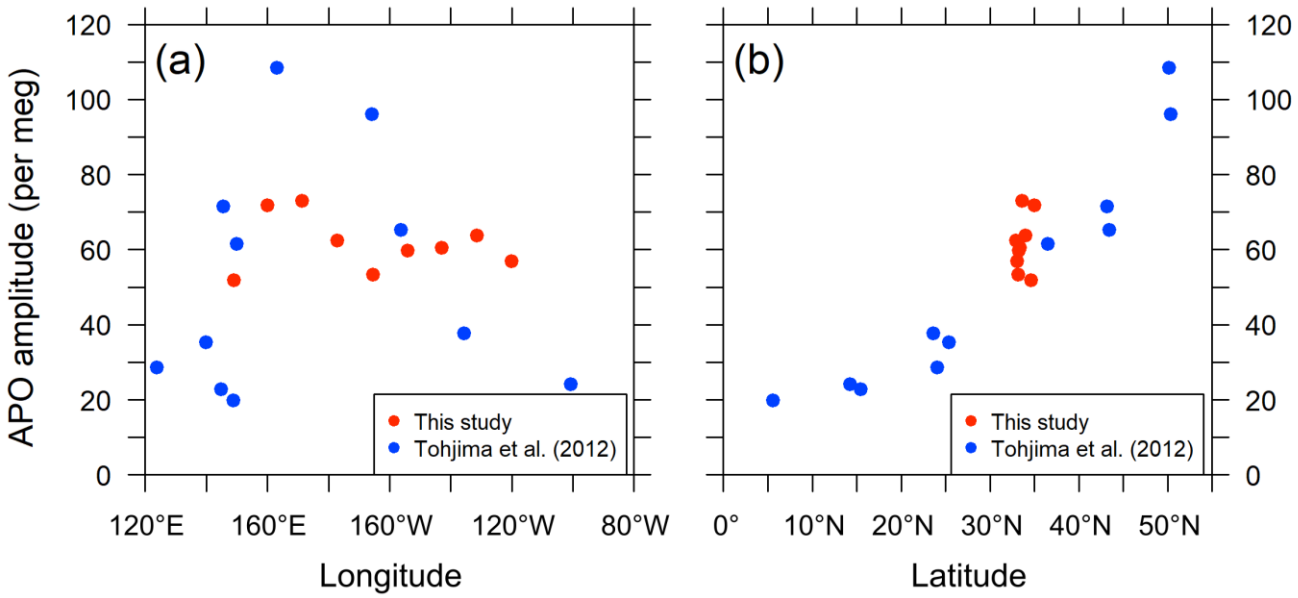

Figure 12: Distribution of seasonal amplitudes of APO along with (left) longitude and (right) latitude in the North Pacific. The red symbols represent APO amplitudes of the *in situ* data of this study for individual longitudinal bins within middle latitudes (29°N–45°N and 140°E–130°W). The blue symbols represent APO amplitudes reported by Tohjima et al. (2012). The longitudes and latitudes of the plots are the average positions of the data within the individual bins.